Face-Centered Cubic Lattice of Spherical Micelles in Block Copolymer/Homopolymer Blends

Yen-Yu Huang,[†] Hsin-Lung Chen,*[,†] and Takeji Hashimoto*[,‡]

Department of Chemical Engineering, National Tsing Hua University, Hsin-Chu, 30013, Taiwan, R.O.C., and Department of Polymer Chemistry, Graduate School of Engineering, Kyoto University, Kyoto 606-8501, Japan

Received March 19, 2002

ABSTRACT: Spherical micelles of block copolymers may arrange into macrolattices in the bulk, in the blends with homopolymers, and in the solutions with low molecular weight solvents. In this study, we present the first experimental observation on the face-centered cubic (fcc) lattice of spherical micelles in diblock copolymer/homopolymer blends based on the blend of a symmetric poly(ethylene oxide)-*block*-poly(1,4-butadiene) (PEO-*b*-PB) and a PB homopolymer. The fcc lattice at elevated temperatures is verified through small-angle X-ray scattering and transmission electron microscopy. The thermally induced phase transition on heating is found to proceed through an order−order transition from body-centered cubic (bcc) to fcc phase followed by an order−disorder transition from fcc packing to disordered micelles and eventually to a homogeneous melt with only thermal concentration fluctuations.

Introduction

Molecular self-assembly in diblock copolymers, A-*b*-B, may generate a series of long-range ordered microdomains depending on the strength of interblock repulsion and composition of the constituting blocks.[1−5] The classical structures include lamellae, cylinder, and sphere, and complex structures such as gyroid phase have also been disclosed.[6−9] The geometry of microdomain formed is largely determined by the competition between the interfacial tension at domain interface and the stress in the stretched chains. The block chains are stretched since the chains confined in the respective domains must satisfy the melt incompressibility that requires the two phases to attain their normal liquid densities.

In highly asymmetric diblock melts, the minority blocks (e.g., B blocks) assemble into spherical microdomains with A blocks tethered to the domain interface, yielding spherical micelles consisting of a core and a coronal shell. These micelles may organize into macrolattices, where a body-centered cubic (bcc) lattice is the only structure observed in bulk so far, although theories have predicted other lattice packings including face-centered cubic (fcc) or hexagonal close-packed (hcp) structures.[10,11] For instance, Matsen and Bates unified the strong and weak segregation limit theories of block copolymers based on the use of self-consistent mean-field (SCMF) theory.[10] A close-packed sphere (CPS) morphology with micelles packed into fcc or hcp lattice was predicted to exist in a narrow region in the phase diagram. According to the phase diagram, an order−disorder transition (ODT) from bcc to disordered phase (free from micelles and with only thermal concentration fluctuations) should be intervened by a CPS phase; however, such a CPS morphology has never been identified unequivocally so far. The absence of CPS phase may be due to the thermal fluctuation effect (i.e., the Brazovskii effect) which intensifies at elevated temperatures.[12,13] The thermal fluctuations may destabilize the long-range order of CPS phase but not spheres themselves, thereby giving rise to disordered micelles before the system attains homogeneous melt (free from micelles and with only thermal concentration fluctuations) with increasing temperature. Existence of the fluctuation-driven disordered micelles was clarified by a series of experimental works by Sakamoto et al.[14−16] and Han et al.[17] A recent theory by Dormidontova and Lodge verifies the above conjecture and asserts that the CPS phase is not thermodynamically stable in neat diblocks if the disordered melt is considered to consist of disordered micelles instead of a homogeneous melt.[18] The stability of the CPS phase is superseded by the disordered micelle regime due to the gain in translational entropy of the micelles.

As the domain structure is closely governed by the composition, block copolymer mesophase may also be tailored by blending with the corresponding homopolymer of one of the blocks (e.g., A-*b*-B/A blends).[19−23] The addition of A homopolymer may cast additional phase behavior onto the system. For instance, existence of the homopolymer in the matrix phase for micelles alleviates the packing frustration of the coronal blocks forming the matrix phase, whereby the coronal chains that must stretch most into the vertexes of the Wigner−Seitz cell can relax upon localization of the homopolymers near the vertexes.[24,25] It has been demonstrated that such a packing frustration is one of the important physical factors associated with the transformation between bcc and CPS phase in sphere-forming blends.[24−27] Nevertheless, the CPS phase with either fcc or hcp packing has also never been observed in A-*b*-B/A blends.

Block copolymer micelles are also formed in the solutions with selective low molecular weight solvents, where interactions between polymer and solvent in the coronal layers plays an important role in micelle ordering in the semidilute and concentrated regimes. fcc lattice in this type of system has been identified in a number of cases.[28−32] McConnell et al. observed the fcc phase over certain concentration range in the solutions of polystyrene-*block*-polyisoprene (PS-*b*-PI) and de-

* To whom correspondence should be addressed.
[†] National Tsing Hua University.
[‡] Kyoto University.

10.1021/ma0204305 CCC: $25.00
Published on Web 01/04/2003

cane.[28] The lattice structures were found to correlate with the ratio of coronal layer thickness to core radius, where a thinner corona favored the formation of an fcc lattice. Pople et al. identified the thermally induced transition between bcc and fcc lattices in the aqueous solutions of poly(oxyethylene)-*block*-poly(oxybutylene).[31] The transition into fcc phase upon heating was postulated to be driven by the decrease in coronal layer thickness due to the poorer solvation of poly(oxyethylene) blocks at higher temperatures. fcc lattice has also been reported recently by Hanley et al. for PS-*b*-PI dissolved in diethyl phthalate, a good solvent for PS but poor for PI.[32]

In this study, we will present the experimental evidence on the existences of fcc lattice, thermally induced bcc−fcc order−order transition (OOT), and ODT from fcc to disordered micelle phase in A-*b*-B/A blends based on the blend of a poly(ethylene oxide)-*block*-poly(1,4-butadiene) (PEO-*b*-PB) and a PB homopolymer. A symmetric PEO-*b*-PB which displayed lamellar morphology in the melt was blended with a PB homopolymer, yielding PEO spherical microdomains in the matrix composed of wet-brush type blends of PB homopolymer and PB blocks tethered at PEO spheres.[33] The macrolattices in the resultant blend will be probed by using small-angle X-ray scattering (SAXS) and transmission electron microscopy (TEM).

Experimental Section

The symmetric PEO-*b*-PB with a polydispersity index (M_w/M_n) of 1.04 was synthesized by sequential anionic polymerization of butadiene and ethylene oxide (Polymer Source, Inc.). M_n of the PEO and PB blocks were 6000 and 5000, respectively. The 1,4-addition PB homopolymer with $M_n = 2600$ and $M_w/M_n = 1.04$ was also synthesized by anionic polymerization (Polymer Source, Inc.). The microphase-separated PEO-*b*-PB/PB blend with the overall volume fraction of PEO, $f_{PEO} = 0.17$, was prepared by solution mixing using toluene as the cosolvent, followed by removing the solvent in vacuo at 80 °C.

Temperature-dependent SAXS measurements were conducted to probe the melt morphology of PEO-*b*-PB/PB blend at various temperatures. The as-cast sample was annealed at 130 °C for 2 h under nitrogen atmosphere prior to the measurement. As will be clarified later, this temperature is the one in which the micelles are ordered in bcc lattice at equilibrium. The SAXS experiments were performed in a heating process under nitrogen atmosphere in a temperature-controlled sample cell described elsewhere.[34] The sample was held at the prescribed temperature for 30 min followed by data acquisition for another 30 min for each measurement. All SAXS profiles were collected above the melting point of PEO to avoid crystallization. Actually, the as-cast sample did not show any detectable trace of crystallinity even after storage at room temperature for 2 months, since crystallization within spherical microdomains has to proceed through homogeneous nucleation which occurs at very deep undercooling (≥90 K).[33,35]

The SAXS apparatus consisted of an 18 kW rotating-anode X-ray generator operated at 30 kV × 400 mA (MAC Science Co, Ltd., Yokohama, Japan), a graphite crystal for incident beam monochromatization, a 1.5 m camera, and a one-dimensional position-sensitive proportional counter. The Cu Kα line ($\lambda = 0.154$ nm) was used. The intensity profiles were output as the plot of the scattering intensity (I) vs the scattering vector, $q = (4\pi/\lambda)\sin(\theta/2)$ (θ = scattering angle). The SAXS profiles were corrected for absorption, air scattering, background scattering arising from thermal diffuse scattering (TDS), and slit-height and slit-width smearing. The intensity level of TDS was assumed to be a constant and its magnitude was determined from the slope of Iq^4 vs q^4 plot at the high-q region ($q > 1.3$ nm^{-1}).[36]

The real-space morphology of the blend was observed by a JEOL JEM-2000FXZ transmission electron microscope operated at 120 kV. The film specimens were microtomed at −90 °C, using a Reichert Ultracut E low-temperature sectioning system. The ultrathin sections were stained with the vapor of 1% OsO_4(aq) for 2 h.

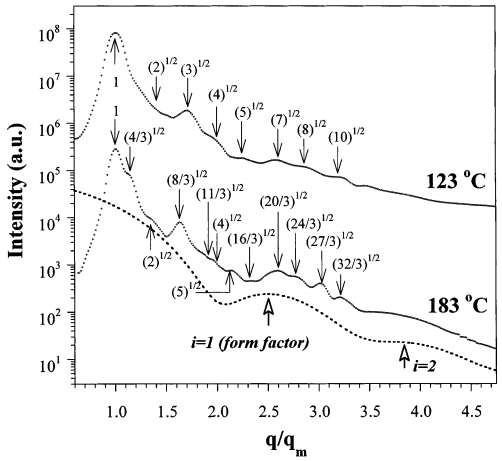

Figure 1. Comparison between the SAXS profiles collected in situ at 183 °C with that measured in situ at 123 °C. The scattering profiles are presented as a function of q/q_m with q_m being the position of the first-order lattice peak at each temperature. The relative positions of the higher order lattice peaks are indexed by the thin arrows, while the form factor peaks (denoted by "$i = n$" with $n = 1, 2, ...$) are indicated by the bold opened arrows. The dotted line signifies the form factor profile of spheres calculated by assuming $\langle R \rangle = 7.5$ nm and the standard deviation of R, $\sigma_R = 0.72$ nm (Gaussian distribution was adopted for R distribution).

Results and Discussion

Figure 1 compares the SAXS profile collected in situ at 183 °C with that measured in situ at 123 °C. The scattering peaks arising from the intermicrodomain interference of the scattered field (designated hereafter as lattice peaks) are marked by thin arrows, while bold opened arrows pinpoint the peaks arising from the form factor scattering (denoted by "i = n" with $n = 1, 2, ...$) from isolated spherical domains.[33,37] The average radius of PEO spheres ($\langle R \rangle$) deduced from the positions of the form factor maxima is 7.5 nm, as the dotted line signifies the form factor profile of spheres calculated by assuming $\langle R \rangle = 7.5$ nm and the standard deviation of R, $\sigma_R = 0.72$ nm (Gaussian distribution was adopted for R distribution). The SAXS patterns at these temperatures are different in terms of the relative positions of the lattice peaks. At 123 °C, the lattice peaks display relative positions closely relevant to bcc symmetry as usually expected. Strikingly different features are identified in the scattering pattern measured at 183 °C, where a shoulder clearly appears beside the first-order lattice peak. The position of this shoulder relative to that of the primary peak is $(4/3)^{1/2}$, which conflicts with the position of any of the higher-order peaks for a bcc lattice. At this temperature, the relative positions of the majority of peaks (labeled in the figure) closely follow those prescribed by a fcc lattice.[38] The SAXS pattern is actually very similar to those reported for the fcc structures in the solutions of PS-*b*-PI with low molecular weight solvents.[28,32] It is noted that the weak shoulders observed near $q/q_m \approx 1.4$ and 2.2 nm^{-1}, not assignable to an fcc lattice, may stem from the presence of residual bcc phase.

In addition to fcc packing, hcp represents the other type of close-packed arrangement. According to the SCMF calculation by Matsen, these two types of lattice

Table 1. Diffraction Planes and Relative Positions of the Lattice Peaks of bcc, fcc, and hcp Lattices

BCC		FCC		HCP	
diffraction plane (*hkl*)	relative position	diffraction plane (*hkl*)	relative position	diffraction plane (*hk·l*)	relative position
(110)	1	(111)	1	(10·0)	1
(200)	$2^{1/2}$	(200)	$(4/3)^{1/2}$	(00·2)	1.06
(211)	$3^{1/2}$	(220)	$(8/3)^{1/2}$	(10·1)	1.13
(220)	$4^{1/2}$	(311)	$(11/3)^{1/2}$	(10·2)	1.46
(310)	$5^{1/2}$	(222)	$4^{1/2}$	(11·0)	1.73
(222)	$6^{1/2}$	(400)	$(16/3)^{1/2}$	(10·3)	1.88
(321)	$7^{1/2}$	(331)	$(19/3)^{1/2}$	(20·0)	2.00
(400)	$8^{1/2}$	(420)	$(20/3)^{1/2}$	(11·2)	2.03
(411),(330)	$9^{1/2}$			(20·1)	2.07
(420)	$10^{1/2}$			(00·4)	2.12
				(20·2)	2.26
				(10·4)	2.34
				(20·3)	2.56
				(21·0)	2.64
				(21·1)	2.70

are essentially degenerate in free energy, and any energy difference is expected to be insignificant in comparison to nonequilibrium effects.[24] The scattering features of hcp lattice are briefly described in the Appendix. Table 1 tabulates the lattice planes and relative positions of the corresponding diffraction peaks for ideal hcp packing. Since the scattering peaks of such a lattice are closely spaced and some of the positions lie in the vicinity to those of the fcc lattice, it may be speculated that a great number of peaks are not resolvable by the SAXS apparatus employed, such that fcc and hcp cannot be distinguished unambiguously. However, judging from the facts that the strong diffraction observed at $q/q_m = (8/3)^{1/2}$ is not closely predicted by hcp lattice and the overall scattering profile at 183 °C is in parallel with that reported for the fcc lattice in diblock copolymer solutions, assigment of the fcc lattice to the system at 183 °C should be justifiable. As a matter of fact, because both fcc and hcp stand for close-packed arrangement and their energy difference is insignificant, it may not be necessary to distinguish between these two rigorously so long as CPS is shown to exist in the blend.

We have also attempted in resolving the real-space structure of the fcc phase through TEM observation. In this experiment, the sample used in the SAXS measurement at 183 °C was rapidly quenched into cold water (the sample was well-sealed in a cell to prevent direct contact with water in the quench process), and the cooled specimen was brought to a cryomicrotome from which the ultrathin sections were prepared. The subsequent room-temperature SAXS characterization of the cooled sample revealed that the fcc peaks still preserved upon immediate cooling (the middle curve in Figure 2), but the scattering maxima tended to diminish and transform into those associated with the bcc lattice upon prolonged annealing at room temperature (as evidenced from emergence of the $(3)^{1/2}$ peak in the bottom curve in Figure 2).

Figure 3 shows the representative TEM micrographs. The dark matrix is the PB phase owing to the preferential staining by OsO_4. The image appears like a double-layer structure with the upper layer consisting of the "bright spheres" and the lower layer containing the "gray spheres" of PEO. The lower layer slips against the upper layer by a distance of about $3^{1/2}a/2 - D = 0.97$ D (where a is the edge length of the unit cell and D is the sphere diameter with the assumption of $D/a =$

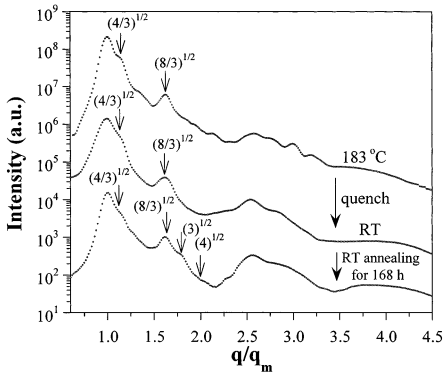

Figure 2. SAXS profiles showing that the fcc phase at 183 °C was not destroyed immediately after cooling to room temperature. Top curve (with $q_m = 0.30$ nm^{-1}): collected in situ at 183 °C. Middle curve (with $q_m = 0.286$ nm^{-1}): collected immediately after cooling to room temperature. Bottom curve (with $q_m = 0.268$ nm^{-1}): collected after annealing the cooled sample at room temperature for 168 h.

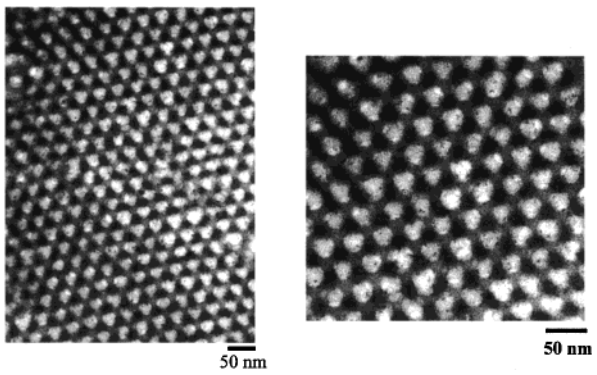

Figure 3. Representative TEM micrographs of PEO-*b*-PB/PB blend ($f_{PEO} = 0.17$) quenched from 183 °C. The dark matrix is the PB phase owing to the preferential staining by OsO_4.

0.44, which corresponds to the sphere volume fraction of 0.18), giving rise to the image resembling the slippage between two (111) planes along the reciprocal lattice vector of (110) plane in the bcc lattice. Nevertheless, since TEM micrograph presents the 2-D projections of the actual lattice structure in the thin-section, straightforward interpretations of the observed image may sometimes be misleading and erroneous. Alternatively, we compare the observed image with that derived from a computer graphics program, TEMS, capable of generating the TEM images projected from arbitrary planes in the macrolattices including bcc and fcc symmetries.[39−41] It is found that the bcc lattice can never generate the image observed in Figure 3. On the other hand, the fcc lattice can yield the observed image (as shown in Figure 4b) if the ultrathin section is cut parallel to (111) planes and the specimen contains two layers (e.g., B and C) of spheres with the spheres in plane B fully contained in the thin section (giving rise to the image of bright spheres) and those in plane C partially contained in the specimen (yielding the image of gray spheres). It should be noted that the agreement between the TEMS image and the observed TEM image alone may not completely rule out other symmetries except for bcc and simple cubic lattice, while a combination of SAXS and TEM results has offered a solid evidence for the existence of the fcc lattice.

The mechanism for the formation of close-packed arrangement is usually rationalized by the relief of packing frustration of coronal block chains.[24,42] In neat

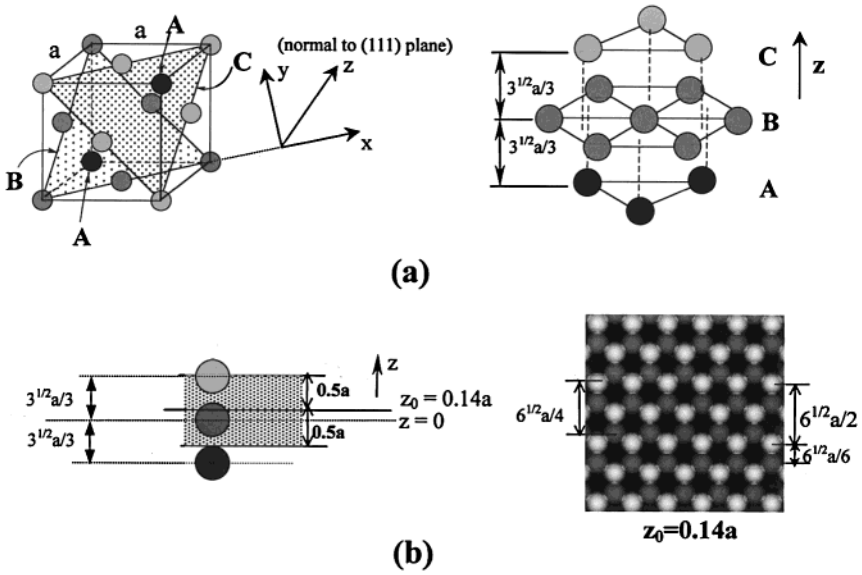

Figure 4. Characteristics of fcc lattice and the TEM image generated by computer graphics. (a) 3-D structure of a fcc unit cell; the edge length of the unit cell is a, and the coordinate is defined in such a way that z axis aligns normal to the (111) plane. The fcc lattice can be built by stacking together (111) planes in a ABCABC... stacking sequence. The spheres in plane B fit over valleys of those in plane A and the spheres in plane C fit over valleys of those in both planes A and B. The distance between two adjacent planes is $(3)^{1/2}a/3$. (b) Computer-generated TEM image for the thin section cut parallel to (111) planes in fcc lattice. The origin of the z axis is defined at the center of the spheres in plane B, and the offset position, z_0, specifies the centerline of the thin section (represented by the shadowed region) relative to the position of $z = 0$. We binarize the contrast of each phase in such a way that the sphere is bright and matrix is dark and then calculate the average contrast of the TEM image of a given thickness. The image consistent with that observed in Figure 3 is generated using the parameters of thin section thickness $= a$, D/$a = 0.44$ (corresponding to the sphere volume fraction of 0.18, being close to the volume fractions calculated from stoichiometry (0.17) and the SAXS peak positions (0.15)), and $z_0 = 0.14a$. In this case, the spheres at plane A are not included in the thin section, so they disappear in the TEM micrograph; the image consists of bright spheres in plane B, gray spheres in plane C, and a dark matrix.

diblocks, stretching of coronal blocks tethered at the spheres is not uniform because a portion of them have to stretch more to fit into the vertexes of Wigner−Seitz cells in the matrix phase to produce a cmc surface under the constraint of melt incompressibility.[42] Such a packing frustration is stronger in a bcc lattice than in a fcc lattice because the corresponding Wigner−Seitz cell in the former is a truncated octahedron while that in the later is a rhombic dodecahedron. Therefore, fcc packing is favored in terms of relief of packing frustration. On the other hand, bcc-packed micelles have a smaller interface-to-volume ratio (S/V with S being the total interfacial area and V being the total volume) under a given sphere volume fraction. Spherical micelles then prefer bcc packing if interfacial energy dominates the relief of packing frustration. This is particularly plausible at low temperatures since the interblock repulsion is strong (i.e., large χ). Increasing temperature or lowering χ tends to alleviate the effect of interfacial tension, where the spheres could split into smaller size (i.e., the association number decreases), thereby allowing them to rearrange into a fcc lattice to release packing frustration.

In A-*b*-B/A blends, the presence of hompoplymer could alleviate packing frustration in that a portion of homopolymer chains may be localized near the vertexes of the Wigner−Seitz cells, thereby permitting the coronal blocks originally reaching the vertexes to relax.[24,25] At low temperatures, repulsive interactions between PEO and PB are strong so that PB coronal blocks tend to behave as dry brushes against homo-PB chains, a part of which can be localized near the vertexes of the Wigner−Seitz cells, thereby relaxing the packing frustration of the coronal chains. This packing frustration is released in both bcc and fcc lattice symmetry. Under a given overall volume fraction of PEO or PB, S/V is smaller in the bcc lattice, and consequently, bcc symmetry is preferred to fcc at low temperatures.

At high temperatures, repulsive interactions between PEO and PB decrease so that PB coronal blocks tend to behave as wet brushes against homo-PB chains. To fill the space near the vertexes of the Wigner−Seitz cells, both the coronal PB and homo-PB chains must be stretched. These packing frustrations are smaller for fcc than for bcc for the same reason as that indicated for neat block copolymers. The same argument as that employed for neat diblocks can be applied also for S/V. Again at high temperatures the effect of releasing packing frustrations outweighs that of increasing S/V, which then stabilizes fcc symmetry rather than bcc symmetry for the PEO-*b*-PB/PB system studied.

Figure 2 demonstrates bcc and fcc structure at 123 and 183 °C, respectively; this implies that a bcc to fcc OOT exists between these two temperatures. Figure 5 displays a series of SAXS profiles measured in situ at various temperatures from 123 to 183 °C. In the figure, we also used reduced scattering vector in order to facilitate to check the thermally induced OOT process where q was reduced with q_m measured at each temperature. At $T \leq 132$ °C, the blend contains exclusively bcc lattice as only the characteristic bcc peaks are observed. Upon further heating, a scattering maximum associated with the $(8/3)^{1/2}$ peak (due to the (220) lattice plane) of the fcc lattice starts to emerge, and the $(3)^{1/2}$ peak of the bcc phase starts to diminish at 135 °C. At 142 °C, a shoulder corresponding to the $(4/3)^{1/2}$ fcc peak (due to the (200) plane) appears beside the primary peak, and the $(8/3)^{1/2}$ maximum becomes dominant over the neighboring $(3)^{1/2}$ bcc peak. The overall scattering profile in this case represents a superposition of the individual patterns from bcc and fcc lattices owing to the coexistence of these two types of structure. The

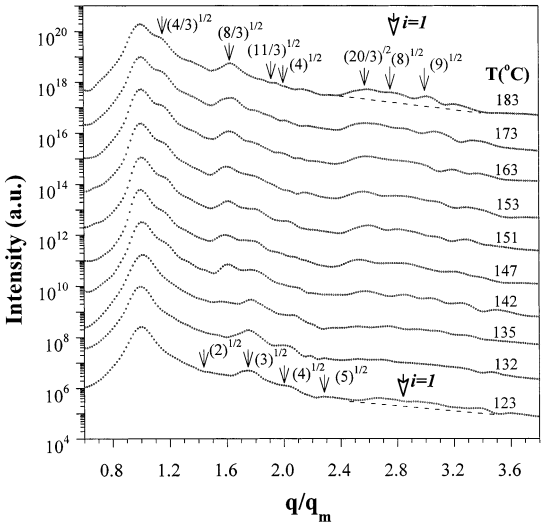

Figure 5. Series of SAXS profiles collected in situ at various temperatures from 123 to 183 °C, showing an OOT from bcc to fcc phase. The total experimental time spent between the SAXS measurement at 135 and that at 163 °C, i.e., the time period over which the bcc symmetry was transformed into the fcc symmetry, was 8 h. The change in q_m with temperature (T) can be evaluated from that in D ($=2\pi/q_m$) with T shown in Figure 7.

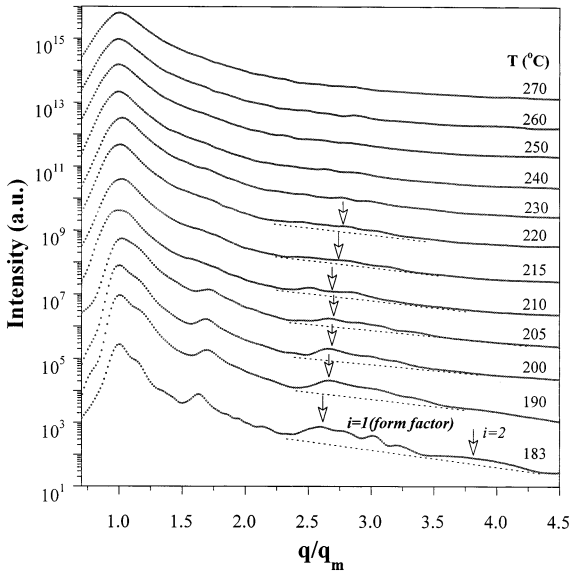

Figure 6. Series of SAXS profiles collected in situ at $T \geq 183$ °C, showing an ODT from fcc phase to disordered micelles followed by demicellization into a homogeneous melt. The same comment as that in Figure 5 is applicable for the change in q_m with T. The background level is drawn by the dashed line to manifest the form factor scattering.

contribution of the bcc phase becomes insignificant at 163 °C where the micelles predominantly pack into a fcc lattice. The SAXS patterns in Figure 5 indicate that the fcc phase tends to grow at the expense of the bcc phase. The transition from the bcc to the fcc lattice is found to occur at temperatures ranging from 135 to 163 °C over the time scale (60 min) associated with each SAXS measurement. The transition range could be narrower if the annealing time at each temperature becomes longer.

At this point it would be of worthy to note a possible reason the bcc−fcc transition was observed for the present PEO-*b*-PB/PB system but not for other bulk systems, such as PS-*b*-PI and its blends with corresponding homopolymers. A PS-*b*-PI (SS-7 in ref 43 or SI-2 in ref 44 with $M_n = 1.9 \times 10^4$, $M_w/M_n = 1.02$, and $f_{PS} = 0.46$) has number-average degree of polymerization $N_n = 220$ similar to the PEO-*b*-PB used here ($N_n = 229$). The PS-*b*-PI has $T_{ODT} = 142$ °C, where the PEO-*b*-PB has $T_{ODT} > 220$ °C, indicating that the latter has a larger χ. Since the strength of thermal noise B is given by $B \sim (\chi N)^{-1/2} N^{-1/2}$,[44,45] for a given N and f_A ($=N_A/(N_A + N_B)$), B is expected to be smaller for PEO-*b*-PB than for PS-*b*-PI, and hence, the fcc phase may be less disturbed by the thermal fluctuation effects for PEO-*b*-PB than for PS-*b*-PI, which may explain the reason pointed out in the beginning of this paragraph.

In addition to the bcc−fcc transition, we are also interested in revealing if further phase transition is accessible at even higher temperatures for the present system. Figure 6 presents a series of SAXS profiles obtained at $T \geq 183$ °C, again plotted against q/q_m. It can be seen that the higher-order lattice peaks and the form factor peak start to diminish on further heating from 183 °C. It should be noted that the form factor peak is a broad scattering peak (labeled by the arrows) appearing above the background level drawn by the dashed line. The ripples superposed on the broad form factor peak may reflect either higher-order lattice diffractions or noise. Only the primary peak is identified along with a broad shoulder at $q/q_m \approx 1.7$ and a weak form factor scattering at 215 °C, indicating the microdomains have lost their long-range order and the system contains disordered micelles.[14−16] These micelles gradually dissociates (through the demicellization process) with increasing temperature, and the form factor peaks become negligible in the SAXS profiles above 220 °C, indicating that the system may have attained a homogeneous state with only thermal concentration fluctuations. It should be noted that the changes of SAXS patterns were by no means due to any chemical reactions that might occur at high temperatures, since the phase transition was thermally reversible in the sense that both lattice and form factor scatterings were recovered upon cooling the sample from 270 °C to room temperature.

The temperature dependences of SAXS patterns in Figures 5 and 6 indicate that the system underwent a bcc−fcc OOT and an ODT from the fcc phase to disordered micelles. It should be noted that this ODT reflects a physical process of the so-called "lattice disordering/ordering transition (LDOT)", as disordered micelles exist at thermal equilibrium for a certain temperature range above the ODT.[14−16] The phase transitions can also be manifested from the plot of the inverse of the intensity maximum (I_m^{-1}) of the primary scattering peak as a function of the inverse of temperature in Figure 7a. The temperature dependence of the characteristic distance ($D = 2\pi/q_m$) is also displayed for comparison. Large discontinuities of I_m^{-1} and D are identified at $T_{LDOT} = 210$ °C, which corresponds to the phase transition from fcc phase to disordered micelles. bcc−fcc OOT is found to generate a small discontinuity (denoted by the solid arrows) in I_m^{-1} near 163 °C, as demonstrated more clearly by the enlarged plot in Figure 7b. A detailed study on the discontinuity across the bcc−fcc OOT is being attempted using ultra-small-angle X-ray scattering (USAXS) which increases the spatial resolution by a factor of about 10 compared with the conventional SAXS camera.[43,46] The inflection point at $T^{-1} \approx 1.95 \times 10^{-3}$ (K^{-1}) or $T \approx 240$ °C in the plot of I_m^{-1} vs T^{-1} above T_{LDOT} shown in Figure 7a might

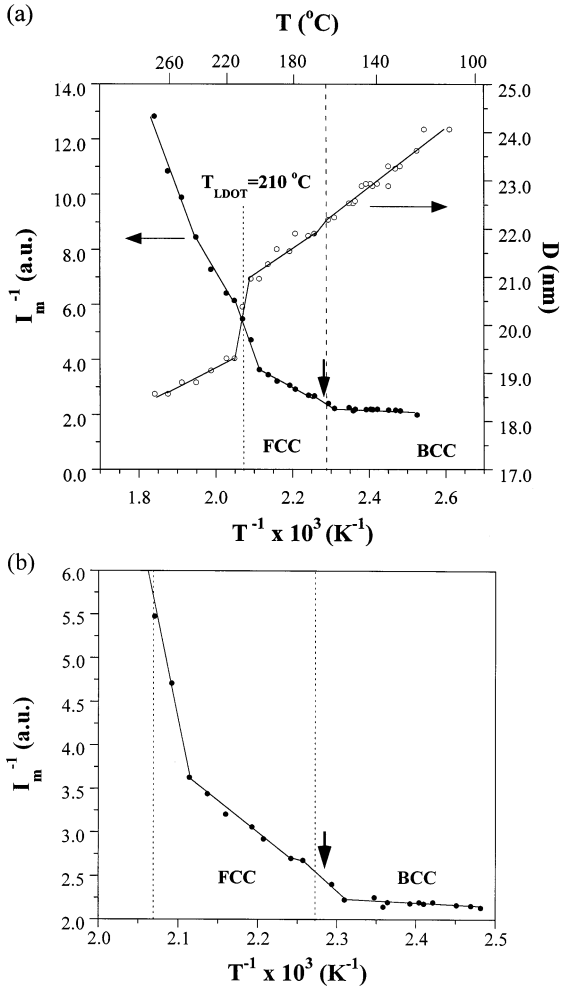

Figure 7. (a) Determinations of the lattice disordering temperature (T_{LDOT}) or ODT from fcc phase to disordered micelle phase from the plots of I_m^{-1} vs T^{-1} and D vs T^{-1} in the heating process. A small discontinuity (denoted by the solid arrows) in I_m^{-1} is also identified across the bcc−fcc OOT, as demonstrated more clearly by the enlarged plot in part b.

reflect a demicellization temperature above which the system may attain a homogeneous melt effectively free from micelles.

Conclusions

We have demonstrated that fcc packing of spherical micelles can exist in block copolymer/homopolymer blends. The fcc phase constitutes a stable structure lying between bcc and disordered micelle phase; consequently, the thermally induced phase transition on heating proceeds through an OOT from a bcc to an fcc phase, followed by an ODT from an fcc to a disordered micelle phase. The existence of an fcc phase is consistent with the mean-field theories prescribing that the stability of CPS phase is enhanced in the diblocks blended with the corresponding homopolymers.[24,25] However, it will be of interest to reveal if the fcc phase can also exist in neat sphere-forming PEO-*b*-PB. This study is currently in progress in our laboratory.

Acknowledgment. This work was supported in part by the National Science Council of the R.O.C. under Grant NSC 91-2216-E-007-001 and also by a Grant-in-Aid for Scientific Research (under Grant No. 12305060-CA) from the Japan Society for the Promotion of Science.

Appendix. Relative Positions of the Diffraction Peaks of the hcp Lattice

fcc and hcp represent the possible types of close-packed arrangement. The hcp lattice is characterized by the packing of spherical micelles in the ABABAB... stacking sequence while the fcc structure corresponds to the ABCABC... stacking (see Figure 4). Verification of the hcp arrangement from the SAXS profile is not as straightforward as that for the cubic cells, since the relative positions of the lattice peaks depend on the axial ratio of the unit cell, c/a.[38] For an ideal hcp lattice of spheres, $c/a = 1.633$, and the corresponding diffraction planes, indexed by ($hk{\cdot}l$), are listed in Table 1 (along with those associated with bcc and fcc structures for comparison).[38] The lattice spacing $d_{(hk\cdot l)}$ is given by the following equation for the hexagonal lattice[38]

$$\frac{1}{d_{(hk\cdot l)}^{\,2}} = \frac{4}{3}\frac{h^2 + hk + k^2}{a^2} + \frac{l^2}{c^2} \qquad (1)$$

Because $d_{(hk\cdot l)} = 2\pi/q_m^{(hk\cdot l)}$ ($q_m^{(hk\cdot l)}$ = position of the corresponding diffraction peak) and $c = 1.633a$, eq 1 can be transformed into the following equation for calculating the relative positions of the lattice peaks associated with the hcp lattice:

$$q_m^{(hk\cdot l)} = \frac{2\pi}{a}\sqrt{\frac{4}{3}(h^2 + hk + k^2) + \frac{l^2}{1.633^2}} \qquad (2)$$

The relative peak positions obtained from eq 2 are shown in Table 1.

References and Notes

(1) Leibler, L. *Macromolecules* **1980**, *13*, 1602.
(2) Hashimoto, T.; Shibayama, M.; Fujimura, M.; Kawai, H. In *Block Copolymers-Science and Technology*; Meier, D. J., Ed.; Harward Academic Publishers: London, 1983.
(3) Hamley, I. W. *The Physics of Block Copolymers*; Oxford University Press: New York, 1998.
(4) Bates, F. S.; Fredrickson, G. H. *Phys. Today* **1999**, *52*, 32.
(5) Aggarwal, S. L. *Polymer* **1972**, *17*, 938.
(6) Thomas, E. L.; Alward, D. B.; Kinning, D. J.; Martin, D. C.; Handlin, D. L.; Fetter, L. J. *Macromolecules* **1986**, *19*, 2197.
(7) Hasegawa, H.; Tanaka, H.; Yamasaki, K.; Hashimoto, T. *Macromolecules* **1987**, *20*, 1651.
(8) Hajduk, D. A.; Harper, P. E.; Gruner, S. M.; Honeker, C. C.; Kim, G.; Thomas, E. L. *Macromolecules* **1994**, *27*, 4063.
(9) Schultz, M. F.; Bates, F. S.; Almdal, K.; Mortensen, K. *Phys. Rev. Lett.* **1994**, *73*, 86.
(10) Matsen, M. W.; Bates, F. S. *Macromolecules* **1996**, *29*, 1091.
(11) Semenov, A. N. *Macromolecules* **1989**, *22*, 2849.
(12) Brazovskii, A. *Soviet Phys. JETP* **1975**, *41*, 85.
(13) Fredrickson, G. H.; Helfand, E. *J. Chem. Phys.* **1987**, *87*, 697.
(14) Sakamoto, N.; Hashimoto, T.; Han, C. D.; Kim, D.; Vaidya, N. Y. *Macromolecules* **1997**, *30*, 1621.
(15) Sakamoto, N.; Hashimoto, T.; Han, C. D.; Kim, D.; Vaidya, N. Y. *Macromolecules* **1997**, *30*, 5321.
(16) Sakamoto, N.; Hashimoto, T. *Macromolecules* **1998**, *31*, 8493.
(17) Han, C. D.; Vaidya, N. Y.; Kim, D.; Shin, G.; Yamaguchi, D.; Hashimoto, T. *Macromolecules* **2000**, *33*, 3767.
(18) Dormidontava, E. E.; Lodge, T. P. *Macromolecules* **2001**, *34*, 9143.
(19) Roe, R. J.; Zin, W. C. *Macromolecules* **1984**, *17*, 189.
(20) Hashimoto, T.; Tanaka, H.; Hasegawa, H. *Macromolecules* **1990**, *23*, 4387.
(21) Nojima, S.; Roe, R. J.; Rigby, D.; Han, C. C. *Macromolecules* **1990**, *23*, 4305.
(22) Tanaka, H.; Hasegawa, H.; Hashimoto, T. *Macromolecules* **1991**, *24*, 240.
(23) Winey, K. I.; Thomas, E. L.; Fetters, L. J. *Macromolecules* **1992**, *25*, 2645.

(24) Matsen, M. W. *Macromolecules* **1995**, *28*, 5765.
(25) Matsen, M. W. *Phys. Rev. Lett.* **1995**, *74*, 4225.
(26) Leibler, L.; Pincus, P. A. *Macromolecules* **1984**, *17*, 2922.
(27) Semenov, A. N. *Macromolecules* **1993**, *26*, 2273.
(28) McConnell, G. A.; Gast, A. P.; Huang, J. S.; Smith, S. D. *Phys. Rev. Lett.* **1993**, *71*, 2102.
(29) Berret, J. F.; Molino, F.; Porte, G.; Diat, O.; Lindner, P. J. *J. Phys. Cond. Matter* **1996**, *8*, 9513.
(30) Diat, O.; Porte, G.; Berret, J. F. *Phys. Rev. B* **1996**, *54*, 14869.
(31) Pople, J. A.; Hamley, I. W.; Fairclough, J. P. A.; Ryan, A. J.; Komanschek, B. U.; Gleeson, A. J.; Yu, G.-E.; Booth, C. *Macromolecules* **1997**, *30*, 5721.
(32) Hanley, K. J.; Lodge, T. P.; Huang, C.-I. *Macromolecules* **2000**, *33*, 5918.
(33) Chen, H.-L.; Wu, J.-C.; Lin, T.-L.; Lin, J. S. *Macromolecules* **2001**, *34*, 6936.
(34) Hashimoto, T.; Kowaska, K.; Shibayama, M.; Suehiro, S. *Macromolecules* **1986**, *19*, 750.
(35) Chen, H.-L.; Hsiao, S.-C.; Lin, T.-L.; Yamauchi, K.; Hasegawa, H.; Hashimoto, T. *Macromolecules* **2001**, *34*, 671.
(36) Medellin-Rodriguez, F. J.; Philips, P. J.; Lin, J. S. *Macromolecules* **1996**, *29*, 7491.
(37) Chen, H.-L.; Li, H.-C.; Huang, Y.-Y.; Chiu, F.-C. *Macromolecules* **2002**, *35*, 2417.
(38) Cullity, B. D.; Stock, S. R *Elements of X-ray Diffraction*; Prentice Hall: Upper Saddle River, NJ, 2001; Chapter 10.
(39) Nishikawa, Y.; Kawada, H.; Hasegawa, H.; Hashimoto, T. *Acta Polym.* **1993**, *44*, 247.
(40) Nishikawa, Y. Interfacial Curvatures of Bicontinuous Phase Structures in Two-Component Polymeric Systems. Ph.D. Thesis, Kyoto University 1999.
(41) Nishikawa, Y.; Hasegawa, H.; Hashimoto, T.; Hyde, S. T. To be submitted for publication.
(42) Matsen, M. W.; Bates, F. S. *J. Chem. Phys.* **1997**, *106*, 2436.
(43) Koga, T.; Koga, T.; Hashimoto, T. *J. Chem. Phys.* **1999**, *110*, 11076.
(44) Hashimoto, T.; Koga, T.; Koga, T.; Sakamoto, N. In *The Physics of Complex Liquids*; Yonezawa, F., Tsuji, K., Kaji, K., Doi, M., Fujiwara, T., Eds.; World Sci.: Singapore, 1988; p 291.
(45) Ohta, T.; Kawasaki, K. *Macromolecules* **1986**, *19*, 2621.
(46) Bonse, U.; Hart, M. *Appl. Phys. Lett.* **1965**, *7*, 238.

MA0204305